Acta Crystallographica Section D
Biological Crystallography
ISSN 0907-4449

Platinum-induced space-group transformation in crystals of the platelet glycoprotein Ibα N-terminal domain

Kottayil I. Varughese,* Zaverio M. Ruggeri and Reha Celikel

Department of Molecular and Experimental Medicine, The Scripps Research Institute, La Jolla, CA 92037, USA

Correspondence e-mail: kiv@scripps.edu

Received 20 October 2003
Accepted 21 November 2003

PDB Reference: monoclinic platelet glycoprotein Ibα N-terminal domain, 1qyy.

This paper is dedicated to the memory of the late Dr Gopinath Kartha (1927–1984), a pioneering crystallographer whose contributions include the triple helical structure of collagen (with Dr G. N. Ramachandran), the structure of ribonuclease A (with Dr David Harker and Dr Jake Bello) and application of anomalous dispersion data for protein structure determination.

The interaction between platelet glycoprotein (GP) Ibα and von Willebrand factor (VWF) is essential for thrombus formation, leading to the arrest of bleeding. The N-terminal domain of GP Ibα, which contains the binding sites for VWF and α-thrombin, crystallized in the tetragonal space group $P4_3$ with one molecule in the asymmetric unit. When the crystals were treated with platinum, the crystals changed their symmetry from tetragonal to monoclinic $P2_1$ with two molecules in the asymmetric unit. The structure of the monoclinic form was solved using two-wavelength platinum anomalous dispersion data. The tetragonal crystal structure was subsequently solved using molecular-replacement techniques using the monoclinic structure as the search model and was refined with 1.7 Å resolution data.

1. Introduction

GP Ib is part of the GP Ib-IX-V complex located on the platelet surface and is composed of two disulfide-linked subunits, GP Ibα and GP Ibβ, which are the products of separate genes (Ware, 1998). GP Ibα is the structurally and functionally dominant subunit of the complex (145 kDa) and associates with GP Ibβ (22 kDa) and GP IX (17 kDa) in a 1:1:1 stoichiometry. GP V (82 kDa) associates with the GP Ib-IX complex in a 1:2 ratio. Human GP Ibα has binding sites for VWF (Nurden & Caen, 1975) and for α-thrombin (Okumura & Jamieson, 1976). It is composed of 610 residues, of which approximately 490 form the large extracytoplasmic portion of the molecule (also known as glycocalicin). This portion contains an approximately 300-residue amino-terminal domain (GP IbαN), which is the subject of this paper, followed by an 186-residue carbohydrate-rich mucin-like domain with numerous O-linked sugars. Both VWF and α-thrombin binding activities reside in the amino-terminal domain and a striking feature of this domain is the presence of leucine-rich repeats, which are found in a large number of seemingly unrelated proteins.

We carried out the structure analysis in the summer of 2002 and subsequently used the structure as a search model for elucidating the configuration of GP IbαN in complex with α-thrombin (Celikel *et al.*, 2003). In the meantime, two other groups reported the structure of GP IbαN at 2.8 Å (Uff *et al.*, 2002) and 1.85 Å resolution (Huizinga *et al.*, 2002). The latter group also reported the structure of GP IbαN in complex with the VWF A1 domain. Here, we present the structure of GP IbαN at 1.7 Å resolution, focusing mainly on the crystallographic aspects, in particular the space-group transformation induced by the incorporation of platinum and the structure elucidation using anomalous dispersion data.

2. Experimental procedures

2.1. Protein purification

The protein was expressed in stably transfected *Drosophila melanogaster* S2 cells (Invitrogen, Carlsbad, CA, USA) and purified to homogeneity. 1 l of cell medium was dialyzed against 25 m*M* Tris pH 8 and the components of the mixture were separated using a Fast-Flow Q column. The fractions obtained from this column were tested with an enzyme-linked immunosorbent assay using a monoclonal antibody, LJ-P3, immobilized at the bottom of plastic wells to capture GP IbαN. Native human VWF and the modulator ristocetin were then added, followed by a rabbit anti-human VWF immunoglobulin conjugated with horseradish peroxidase to detect the bound VWF. The fractions with GP IbαN activity were then pooled, dialyzed against 25 m*M* Tris pH 8 and digested with *N*-glycanase to remove the N-linked sugar chains. GP IbαN was separated from *N*-glycanase using a DEAE column. The fractions containing GP IbαN were pooled, dialyzed against 25 m*M* Tris pH 8 and passed through a Mono Q column as the last step in the purification scheme.

2.2. Crystallization and data measurement

GP IbαN was crystallized using the hanging-drop technique by mixing equal volumes of protein stock and reservoir solution consisting of 12%(*w*/*w*) PEG 6000, 120 m*M* sodium acetate and 200 m*M* sodium nitrate pH 5.6. The crystals grew in about a week and belonged to the tetragonal space group $P4_3$, with unit-cell parameters $a = 51.73$, $c = 114.04$ Å and one molecule per asymmetric unit. We collected 1.7 Å data on beamline 11-1 at the Stanford Synchrotron Radiation Laboratory using the *Blu-Ice* program (McPhillips *et al.*, 2002). A total of 127 images were measured by rotating the crystal through 1° for each frame. The diffraction data were reduced and scaled using *DENZO* and *SCALEPACK* (Otwinowski & Minor, 1997). The statistics of data collection are given in Table 1.

In order to determine the binding of heavy-atom compounds to the protein, we performed a gel-shift assay with various heavy-metal compounds. Hg, Pt and U compounds [$K_2Pt(NO_2)_4$, $K_2Pt(CNS)_6$, $Hg(CNS)_2$, *para*-chloromercuribenzoate and uranium oxyacetate] caused distinct mobility changes of GP IbαN in native gels. Hence, most of our attempts were to incorporate Pt, Hg and U into the crystal lattice. None of the Hg compounds produced any useful derivatives. Incorporation of platinum and uranium into the crystal lattice generally resulted in significant elongation of the *c* axis and consequent non-isomorphism. The most drastic changes were observed when the crystals were soaked in 30 m*M* $K_2Pt(NO_2)_4$ for two weeks. The space group of the crystals in fact changed from $P4_3$ ($a = 51.73$, $c = 114.04$ Å) to $P2_1$ ($a = 51.6$, $b = 114.3$, $c = 56.3$ Å, $\beta = 94.7°$) with two molecules in the asymmetric unit.

We collected two-wavelength anomalous dispersion data to 2.7 Å using the monoclinic crystal. Measurements were carried out at the peak wavelength and at a remote wavelength employing inverse-beam techniques at the Stanford Synchrotron Radiation Laboratory on beamline 1-5. A total of 360 images, 0–180° and 180–360°, were measured at both energy levels with 1° rotation for each frame in 30° wedges. The data were processed using *MOSFLM* (Leslie, 1987). The data-collection statistics are provided in Table 2. The $\Delta f'$ and $\Delta f''$ values at the two wavelengths were derived from X-ray fluorescence spectra using the program *CHOOCH* (Evans & Pettifer, 2001).

Table 1
Data-collection and refinement statistics for the tetragonal form of GP IbαN.

Values in parentheses are for the highest resolution shell.

(*a*) Data collection and refinement statistics.

Space group	$P4_3$
Unit-cell parameters (Å)	$a = 51.73$, $c = 114.04$
Data collection	Stanford Synchrotron Radiation Laboratory
Wavelength (Å)	1.0642
Detector	Quantum 4 CCD (ADSC)
Data reduction	*DENZO*
No. observations	160737
Unique reflections	31316
Multiplicity of observation	5.1
Refinement	
Protein atoms	2078
Polysaccharide atoms	50
Water O atoms	207
Resolution range for refinement (Å)	10–1.7
No. of reflections in the working set	29109
No. of reflections in the test set	1521
R factor (%)	20.6 (28.3)
R_{free} (%)	22.5 (27.7)
R.m.s. deviations	
Bond lengths (Å)	0.004
Bond angles (°)	1.3
Ramachandran plot	
Residues in most favored regions	174
Residues in additionally favored regions	50
Residues in generously allowed regions	2
Residues in disallowed regions	2

(*b*) Refinement statistics in resolution shells.

Shell (Å)	$I/\sigma(I)$	R_{sym}†	Completeness
50.00–3.66	24.9	0.038	94.2
3.66–2.91	21.2	0.051	99.5
2.91–2.54	23.2	0.056	99.6
2.54–2.31	24.1	0.065	99.4
2.31–2.14	14.1	0.088	99.3
2.14–2.02	11.4	0.126	99.0
2.02–1.91	8.6	0.168	98.9
1.91–1.83	7.4	0.240	98.7
1.83–1.76	7.0	0.285	91.9
1.76–1.70	5.3	0.317	73.6
All reflections	19.8	0.061	95.4

† $R_{sym} = (\sum_h \sum_i |I_{hi} - \langle I_h \rangle|)/\sum_h \langle I_h \rangle$, where I_{hi} is the scaled intensity of the *i*th measurement of reflection *h* or its equivalent and $\langle I_h \rangle$ is the average intensity of reflection *h*.

3. Anomalous scattering and the structure solution of the monoclinic form

Anomalous scattering generally introduces only small changes in intensities, but has now emerged as a very powerful tool in

Table 2
Data-collection and refinement statistics for the monoclinic crystal.

Values in parentheses are for the highest resolution shell.

(*a*) Data-collection and refinement statistics.

Space group	$P2_1$
Unit-cell parameters (Å, °)	a = 51.61, b = 113.82, c = 56.21, β = 95.21
Data collection	Stanford Synchrotron Radiation Laboratory beamline 1-5
Detector	Quantum 4 CCD (ADSC)
Data reduction	*MOSFLM*
Refinement	
Protein atoms	4156
Polysaccharide atoms	64
Water O atoms	56
Pt atoms	3
Resolution range for refinement (Å)	15–2.8
No. reflections in the working set	14556
No. reflections in the test set	741
R factor (%)	22.01 (31.8)
$R_{\rm free}$ (%)	28.21 (37.7)
R.m.s. deviations	
Bond lengths (Å)	0.007
Bond angles (°)	1.5
Ramachandran plot	
Residues in most favored regions	297
Residues in additionally favored regions	140
Residues in generously allowed regions	14
Residues in disallowed regions	5

(*b*) Refinement statistics in shells for λ = 1.071564 Å. f' = −19.2 e, f'' = 13.3 e$^-$. No. of observations = 118 489. Redundancy = 7.0.

$d_{\rm min}$ (Å)	$R_{\rm sym}$	$R_{\rm anom}$†	$I/\sigma(I)$	Completeness (%)	$N_{\rm ref}$
8.54	0.041	0.074	13.5	99.7	589
6.04	0.043	0.073	13.5	99.9	1054
4.93	0.048	0.069	12.8	99.9	1351
4.27	0.049	0.055	12.8	99.9	1578
3.82	0.054	0.053	12.0	99.9	1808
3.49	0.075	0.061	8.8	99.9	1951
3.23	0.113	0.073	6.2	100.0	2170
3.02	0.173	0.092	4.2	99.9	2331
2.85	0.244	0.134	3.0	91.0	2211
2.70	0.317	0.188	2.2	72.2	1889
Overall	0.070	0.069	8.7	94.6	16932

(*c*) Refinement statistics in shells for λ = 1.0079675 Å. f' = −7.9 e$^-$, f'' = 9.2 e$^-$. No. observations = 129 824. Redundancy = 7.3.

$d_{\rm min}$ (Å)	$R_{\rm sym}$	$R_{\rm anom}$†	$I/\sigma(I)$	Completeness (%)	$N_{\rm ref}$
8.54	0.034	0.055	15.5	99.9	589
6.04	0.036	0.052	17.8	100.0	1057
4.93	0.040	0.049	16.2	100.0	1355
4.27	0.041	0.037	15.5	99.8	1580
3.82	0.047	0.037	14.1	99.9	1812
3.49	0.062	0.043	11.1	99.9	1973
3.23	0.090	0.051	7.9	99.4	2176
3.02	0.136	0.069	5.4	94.9	2341
2.85	0.206	0.088	3.5	99.9	2445
2.70	0.257	0.128	2.8	92.2	2411
Overall	0.061	0.049	10.2	98.8	17781

† $R_{\rm anom} = \sum(|I^+ - I^-|)/\sum|I^+| + \sum|I^-|$.

crystal structure analysis. When the incident wavelength of X-rays is close to an absorption edge, the scattering factor of an atom is modified by a dispersion component and an absorption component: $f = f_0 + \Delta f' + i\Delta f''$, where f_0 is the normal scattering factor of the atom as if all electrons are free and $\Delta f'$ and $\Delta f''$ the dispersion and absorption components, respectively. Both the dispersion and the absorption components affect the intensities of Bragg reflections and these intensity variations have been effectively exploited in a number of crystal structure determinations.

More than seven decades ago, Coster *et al.* (1930) observed that the intensities of reflections h, k, l and $-h$, $-k$, $-l$ are not equivalent in the presence of anomalous scatterers. Bijvoet and coworkers (Peerdeman *et al.*, 1951; Bijvoet, 1949) showed that this inequality could be used for the unique determination of the absolute configuration of the molecule and for estimation of phases. In 1956, Ramachandran and Raman worked out a formula for determining the phases of the reflections from the measured Bijvoet differences (Ramachandran & Raman, 1956). Later, Rossmann showed that heavy-atom positions can be located from a Patterson map using the square of anomalous structure-factor differences $|\Delta F|^2$ as coefficients (Rossmann, 1961). This was followed by the work of Kartha and Parthasarathy on anomalous differences in order to obtain a better estimate of the heavy-atom contributions, formulated as $FH^2 = |\Delta F_{\rm iso}|^2 + |\Delta F_{\rm ano}|^2$ (Kartha & Parthasarathy, 1965). Kartha successfully used this formulation to refine heavy-atom positions in ribonuclease (Kartha, 1965). The utility of the anomalous data was further demonstrated when it was combined with isomorphous phases. The non-centric phases estimated from single isomorphous replacement has a twofold ambiguity; however, it can be resolved when combined with anomalous dispersion data (Blow & Rossmann, 1961; North, 1965; Matthews, 1966). The structure of flavodoxin was elucidated from a single isomorphous derivative by resolving the phase ambiguity with anomalous scattering from a single Sm atom (Watenpaugh *et al.*, 1972).

Another important step was the utilization of the dispersion component $\Delta f'$ for phase determination. As $\Delta f'$ varies as a function of energy of the incident beam, by suitable choice of two wavelengths a perfect isomorphism can artificially be created and phase solution can be achieved using exactly the same formulation as isomorphous replacement (Pepinsky & Okaya, 1956; Ramaseshan & Venkatesan, 1957; Mitchell, 1957).

Argos & Mathews (1973) have also shown that although anomalous differences are generally small, they provide useful phasing information. The most spectacular demonstration of the power of anomalous dispersion was the solution of the crambin (4.72 kDa) structure by Hendrickson & Teeter (1981) using the anomalous scattering of sulfur. More recently, Wang and coworkers (Liu *et al.*, 2000) solved a larger protein, obelin (22.2 kDa), using sulfur scattering. However, sulfur anomalous scattering has found only limited application so far in protein structure solution owing to the weak signals of sulfur. In recent years, selenium, a better anomalous scatterer than sulfur, has became the element of choice because of the ease of producing recombinant selenomethionine proteins. With the availability of synchrotron beamlines with tunable energy, anomalous dispersion has now become a widely used technique.

Table 3
Positional and thermal parameters of the Pt atoms.

	X	*Y*	*Z*	*B*	Occupancy
Pt1	−0.192	−0.396	−0.125	55.4	1.0
Pt2	−0.664	−0.647	−0.296	58.7	1.0
Pt3	−0.667	−0.887	−0.469	60.7	0.8

4. Phase solution using platinum anomalous signals

Anomalous difference Patterson maps were computed using the data sets at the peak and remote wavelengths with the program package *PHASES* (Furey & Swaminathan, 1997). In addition, the isomorphous difference Patterson map between the two data sets was also computed. The interatomic vectors of the peak Patterson are stronger on average compared with the remote map, reflecting the magnitude of the dispersion-component peak (Table 2). The peaks in the isomorphous difference Patterson map are weaker than the anomalous maps. The Harker section $v = \frac{1}{2}$ of the peak Patterson map is displayed in Fig. 1(*a*) and the Harker peaks arising from the three Pt atoms are marked 1, 2 and 3. In addition to the three Harker peaks corresponding to interactions between symmetry-related Pt atoms, there is also a strong peak corresponding to the vector between the first and third Pt atoms (Table 3) in this section. The vector corresponding to Pt1→Pt2 interaction falls in the $v = 0.25$ section (Fig. 1*b*) and the Pt2→Pt3 interaction falls in the $v = 0.24$ section (Fig. 1*c*). Because of the strong anomalous signals of platinum, locating the Pt atoms and thus obtaining the phases was straightforward. Three Pt atoms were located using the program *SOLVE* (Terwilliger & Berendzen, 1999) and are listed in Table 3. These positions are consistent with the peaks in the Harker sections.

Protein phases to 3.2 Å were calculated using *SOLVE* (Terwilliger & Berendzen, 1999) and had an overall figure of merit of 0.47. Solvent-flattening calculations were carried out using *RESOLVE* (Terwilliger, 2000) and enhanced the figure of merit to 0.68; the resultant map was of high quality, revealing both molecules entirely except for a few disordered residues.

Model building and refinement were carried out using the program *O* (Jones *et al.*, 1991) and the *CNS* suite of programs (Brünger *et al.*, 1998), respectively. The model was refined to an *R* factor of 22% using 2.8 Å diffraction data; the refinement statistics are provided in Table 2. At this stage, the phasing powers of the three individual components that contribute to phasing were computed using the program package *BNP* (Weeks *et al.*, 2002) and are shown in Fig. 2. The phasing power is computed as a ratio of the heavy-atom contribution (anomalous or isomorphous) to the lack-of-closure error. The phasing power arising from the isomorphous difference is low consistent with the $R_{\rm iso}$ of 2.23%. [$R_{\rm iso}$ is estimated as $\sum(|F_1 - F_2|)/(\sum|F_1| + \sum|F_2|)$.] The anomalous signal present in the data was estimated as $R_{\rm ano} = \sum(|F^+ - F^-|)/(\sum|F^+| + \sum|F^-|)$ for the peak (4.66%) and remote (3.43%) wavelengths. It was surprising that the anomalous data at the two energy levels gave rise to very similar phasing statistics even though the absorption component and the anomalous signal at the remote wavelength are only around 70% of those at the peak wavelength. A closer examination of the diffraction data revealed that the data at the remote wavelength are measured with greater precision.

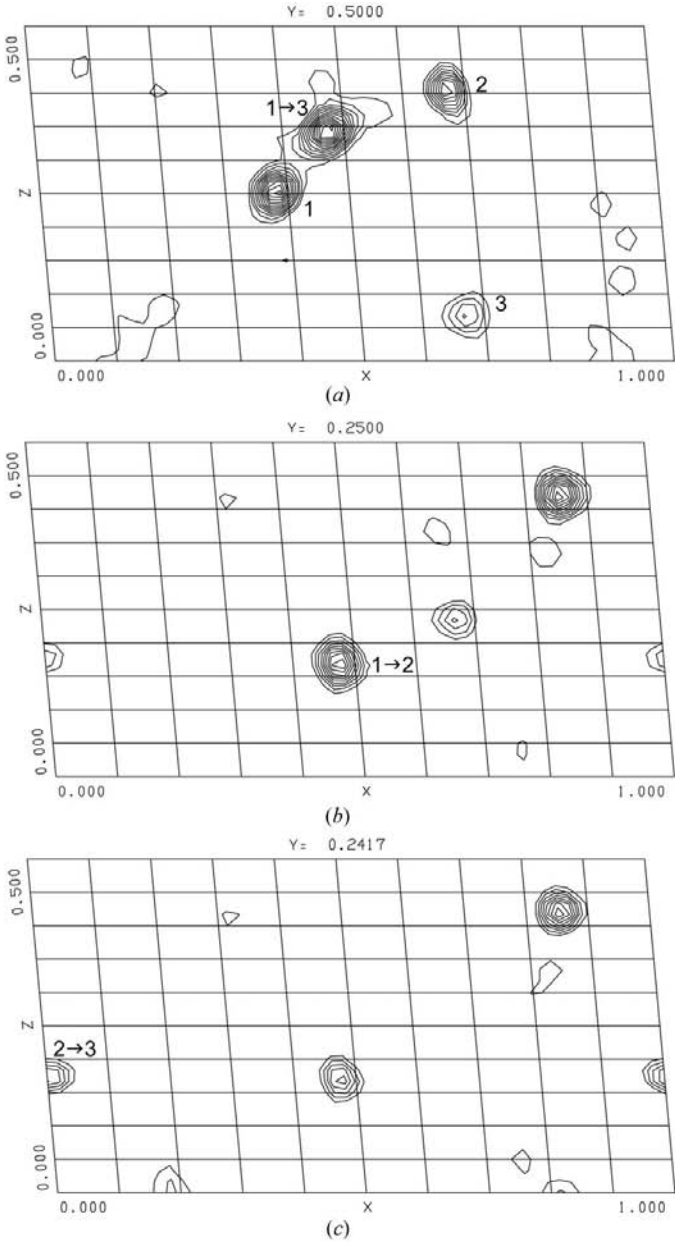

Figure 1
The anomalous difference Patterson at the map peak wavelength (f'' = 13.3e). The contours are at increments of 1σ starting at 2σ. (*a*) The Harker section $v = \frac{1}{2}$. The Harker peaks for the three Pt atoms are denoted 1, 2 and 3. The non-Harker peak between Pt1 and Pt3 also falls in this section and is marked 1→3. The Harker peaks are between the symmetry-related atoms in the two asymmetric unit and have a multiplicity of 1, while the 1→3 interactions arise from both asymmetric units and have a multiplicity of 2. In the monoclinic system, the Harker peaks are at ($u = 2x$, $v = \frac{1}{2}$ and $w = 2z$) and the *x* and *z* values of the three Pt atoms are estimated from this relationship. As $P2_1$ is a polar space group, the *y* coordinate of one of the Pt atoms (say Pt1) can be arbitrarily assigned and the *y* coordinates of Pt2 and Pt3 can be assigned from 1→2, 1→3 and 2→3 interactions. (*b*) $v = 0.25$ section showing the 1→2 interaction. (*c*) $v = 0.24$ section showing the 2→3 interaction.

Despite the treatment of the protein with *N*-glycanase, residue Asn159 stays partially glycosylated with four sugar residues NAG-NAG-MAN-MAN (NAG, *N*-acetyl D-glucosamine; MAN, α-D-mannose) in molecule 1 and only one NAG residue for molecule 2. Fifty-six water molecules with well resolved peaks in the electron-density map were also included in refinement.

4.1. Structure solution (tetragonal form)

The structure of the tetragonal form was solved by molecular-replacement techniques with the *CNS* suite of programs using the monoclinic structure as the search model. Model building was carried out using the program *O* (Jones *et al.*, 1991). The refinements were carried out with 1.7 Å diffraction data using *CNS* and the final *R* factor was 20.6%.

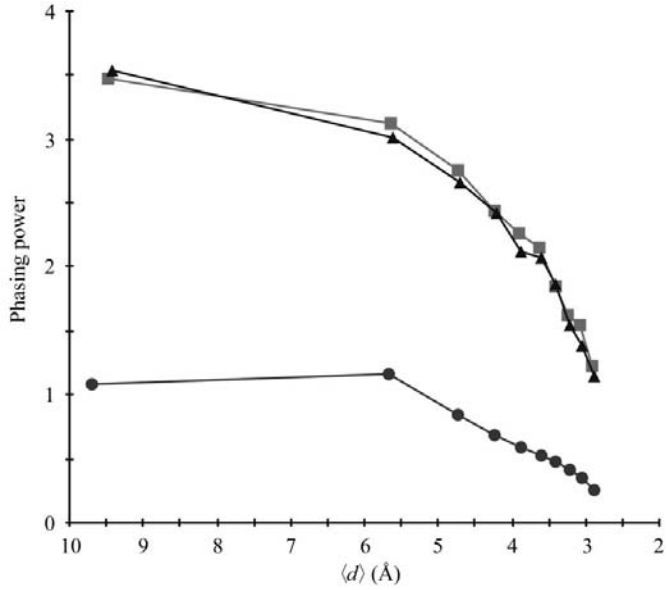

Figure 2
Phasing power computed as function of resolution. Friedel pairs measured at the peak wavelength (squares), Friedel pairs at the remote wavelength (triangles) and the artificial isomorphism arising from the dispersion component (circles) for phase solution.

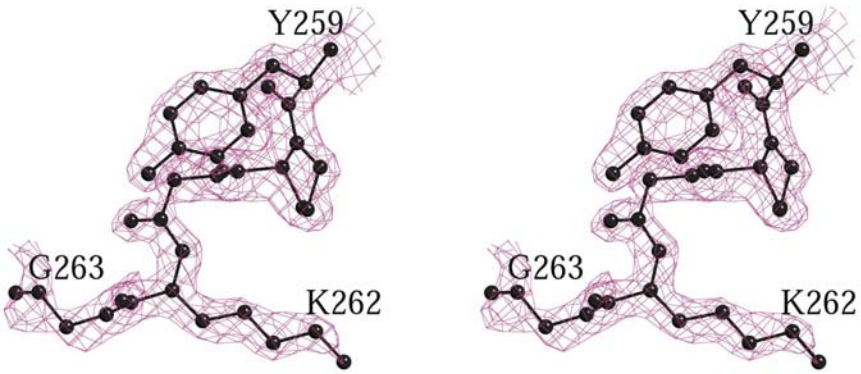

Figure 3
A stereoview of a $2F_o - F_c$ electron-density map of the tetragonal crystal at 1.7 Å. The contours are drawn at the 1.25σ level around the C-terminal residues Tyr259, Pro260, Gly261, Lys262 and Gly263.

This crystal form has only one molecule in the asymmetric unit (Fig. 3). The model consisted of 2078 protein atoms for residues 1–266, 50 polysaccharide atoms of four sugar residues attached to Asn159 and 207 solvent O atoms. A Ramachandran plot shows that 98.2% of the residues fall into most favored or additionally allowed regions, while 0.9% fall into generously allowed regions and 0.9% fall into disallowed regions.

4.2. Tetragonal to monoclinic transformation

Three Pt atoms are incorporated into the asymmetric unit. Two Pt atoms bind to His86 and His195 in one molecule and the third binds to His86 in the other molecule, inevitably breaking the tetragonal symmetry. His86 is situated on the concave surface of the molecule and the C-terminal end of the adjacent molecule packs against this region, placing the Pt atom at the interface between the two molecules. The packing arrangements of the molecules are nearly identical in both forms and Pt appears to cause only minor perturbations in the orientations of the molecules. The binding of the three Pt atoms on the two protein molecules is shown in Fig. 4.

5. Description of the structure

A stereoview of the 1.7 Å resolution structure of GP IbαN is depicted in Fig. 5. The overall structure of the molecule is the same as described previously (Uff *et al.*, 2002; Huizinga *et al.*, 2002). GP IbαN is a member of the leucine-rich repeat (LRR) family of proteins. The N-terminal residues 4–17 form a β-hairpin with a disulfide bridge between residues 4 and 17. It is followed by eight leucine-rich repeats (residues 19–204), which stack upon each other to give a concave surface made up of parallel β-strands. The residues beyond these leucine-rich repeats form a C-terminal cap containing two disulfide bridges between 209 and 248 and between 211 and 264. Residues Ile213–Asn223 form an α-helix and residues Val227–Ser241 form a large loop that plays a critical role in binding the VWF A1 domain. In the complex with the A1 domain, these residues adopt an antiparallel β-strand arrangement and form strong hydrogen bonds with a β-strand of VWF A1 (Huizinga *et al.*, 2002). Residues beyond 264 form a tail that contains three sulfated tyrosine residues Tyr276, Tyr278 and Tyr279 that are crucial for thrombin binding; however, in the present structure residues beyond 266 are not visible.

Two other groups (Uff *et al.*, 2002; Huizinga *et al.*, 2002) have also independently analyzed the structure of GP IbαN. Fig. 6 is a superposition of the present structures with those from the other groups. In general, the eight leucine-rich repeats from the seven individual molecules superpose well; certain other regions, however, exhibit significant flexibility. For example, residues 7–13 in the β-hairpin and residues

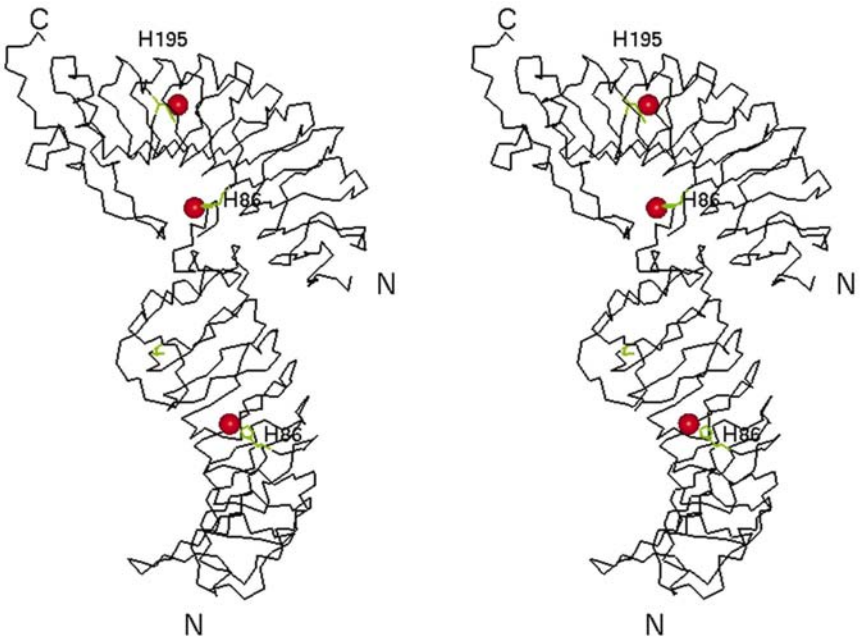

Figure 4
Platinum binding to the two protein molecules in the monoclinic crystal. Pt atoms are shown as red spheres. The histidine residues to which they are bonded are labeled.

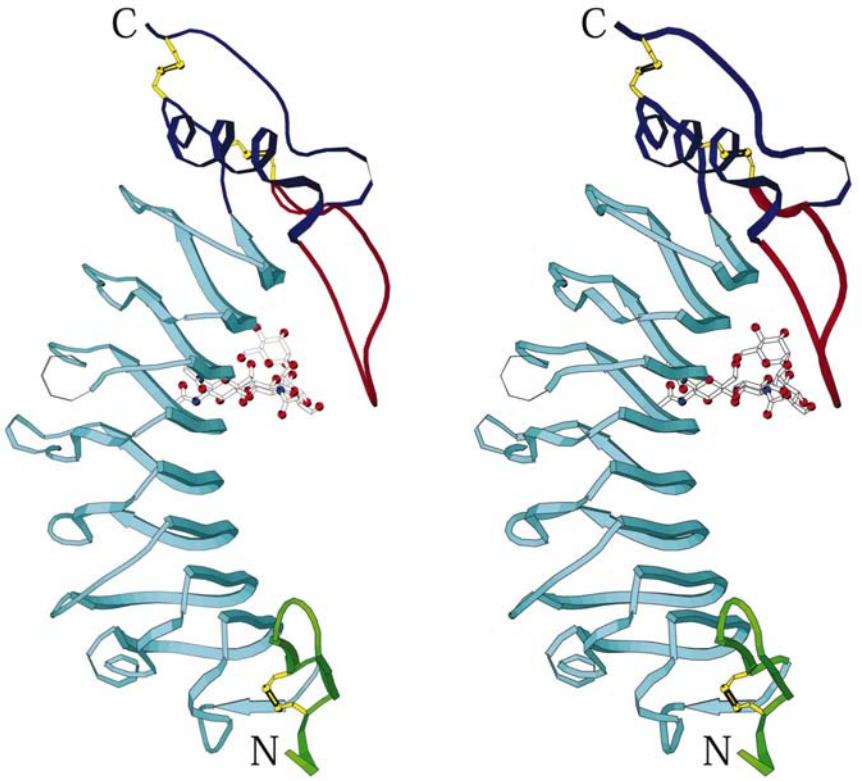

Figure 5
A stereoview of the ribbon diagram of GP Ibα N. The N-terminal β-hairpin is shown in green. The eight leucine-rich repeats are shown in cyan. The consensus motif for leucine-rich repeats usually consists of 24 residues, with leucines predominantly occupying positions 2, 5, 7, 12, 15, 20 and 23. The remaining C-terminal residues containing two disulfide bonds are shown in blue except for the flexible loop (227–242), which is shown in red. This flexible loop participates in A1 VWF binding (Huizinga *et al.*, 2002). The three disulfide bonds (4–17, 209–248 and 211–264) are shown in yellow. The N- and C-termini are marked N and C, respectively.

230–240 in the large flexible loop show considerable variation. The conformations of residues 249–254 fall into two broad types.

6. Mutations in GP Ibα-N structures

The present molecule contains a single mutation Cys65Ala, whereas this residue was not mutated in the other two structures (Uff *et al.*, 2002; Huizinga *et al.*, 2002) depicted in Fig. 6. The mutation does not introduce any conformational changes in the backbone of the molecule and in fact the $C^{\alpha}-C^{\beta}$ bond has the same orientation in all seven of the molecules depicted in Fig. 6. We introduced this mutation to eliminate the dimerization of the wild-type protein and it was surprising that the Cys side chain points into the interior of the molecule. Hence, disulfide formation between two molecules should involve a local conformational change that exposes the Cys side chain.

Two residues, Asn21 and Asn159, are glycosylated in the human protein. The present molecule was expressed in *Drosophila* and treated with *N*-glycanase. Although no sugar residues are seen attached to Asn21, four sugar residues attached to Asn59 are visible. In the structure of Huizinga *et al.* (2002), these two Asn residues are mutated to Gln residues and are devoid of sugars. In the structure of Uff *et al.* (2002), Asn159 has one NAG residue attached in both molecules in the asymmetric unit and has one residue of 2-(acetylamino)-2-deoxy-α-D-glucopyranose attached to Asn21 in one molecule. The local conformations around these two residues are the same in all molecules depicted in Fig. 6.

7. Conclusions

A comparison of our GP Ibα-N structures with the structures reported by the other two groups shows that this domain has a fairly rigid structure. The side chain of residue Cys65 points to the interior of the molecule and its involvement in disulfide formation is an indication of the dynamic flexibilities of the leucine-rich repeat regions. Outside the leucine-rich repeat region, the 227–242 loop, the 249–254 region and the N- and C-termini exhibit considerable flexibility.

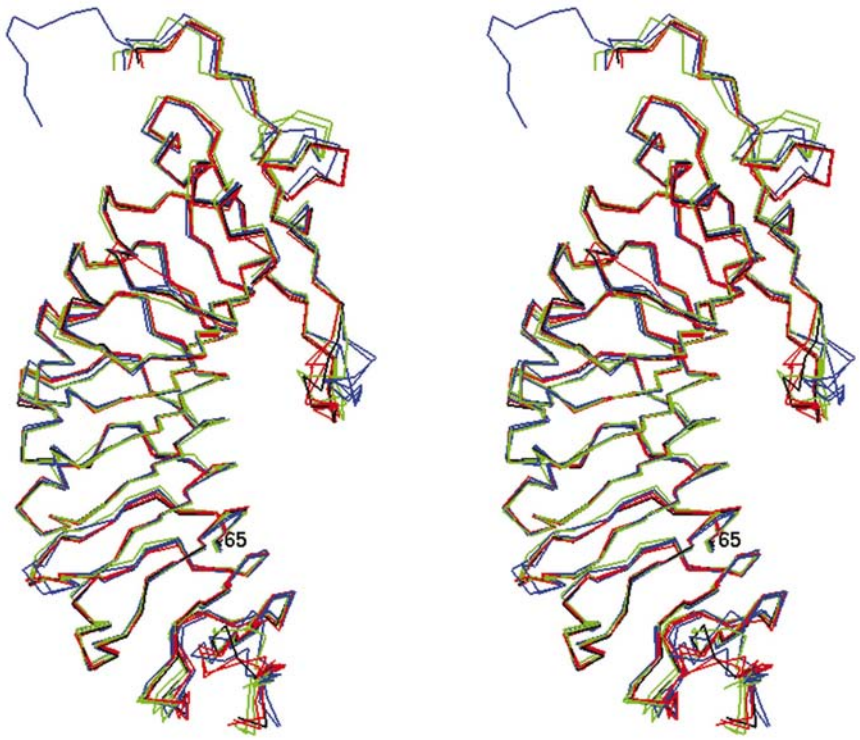

Figure 6
A stereoview of the superposition of GP Ibα N structures. The molecule from the tetragonal crystal is shown in black, the two molecules of the monoclinic crystal in red, the two molecules of Huizinga *et al.* (2002) in green and the molecules of Uff *et al.* (2002) in blue. Cys65 has been mutated to Ala in our structure and is marked 65.

This work was supported by National Institutes of Health grants HL-54246 and HL-42846. We thank the Stanford Synchrotron Radiation Laboratory for beam time and Dr Irimpan Mathews for help with data collection.

References

Argos, P. & Mathews, F. S. (1973). *Acta Cryst.* B**29**, 1604–1611.
Bijvoet, J. M. (1949). *Proc. Koninkl. Ned. Akad. Wet. B*, **52**, 313–314.
Blow, D. M. & Rossmann, M. G. (1961). *Acta Cryst.* **14**, 1195–1202.
Brünger, A. T., Adams, P. D., Clore, G. M., DeLano, W. L., Gros, P., Grosse-Kunstleve, R. W., Jiang, J. S., Kuszewski, J., Nilges, M. & Pannu, N. S. (1998). *Acta Cryst.* D**54**, 905–921.
Celikel, R., McClintock, R. A., Roberts, J. R., Loredana, G., Mendolicchio, G. L., Ware, J., Varughese, K. I. & Ruggeri, Z. M. (2003). *Science*, **301**, 218–221.
Coster, D., Knol, K. S. & Prins, J. A. (1930). *Z. Phys.* **63**, 345–369.
Evans, G. & Pettifer, R. F. (2001). *J. Appl. Cryst.* **34**, 82–86.
Furey, W. & Swaminathan, S. (1997). *Methods Enzymol.* **277**, 590–620.
Hendrickson, W. A. & Teeter, M. M. (1981). *Nature (London)*, **290**, 107–113.
Huizinga, E. G., Tsuji, S., Romijn, R. A. P., Shiphorst, M. E., de Groot, P. G., Sixma, J. J. & Gros, P. (2002). *Science*, **297**, 1176–1129.
Jones, T. A., Zou, J. Y., Cowan, S. W. & Kjeldgaard, M. (1991). *Acta Cryst.* A**47**, 110–119.
Kartha, G. (1965). *Acta Cryst.* **19**, 883–885.
Kartha, G. & Parthasarathy, R. (1965). *Acta Cryst.* **18**, 745–749.
Leslie, A. G. W. (1987). *Proceedings of the CCP4 Study Weekend. Computational Aspects of Protein Crystal Data Analysis*, edited by J. R. Machin & M. Z. Papiz, pp. 39–50. Warrington: Daresbury Laboratory.
Liu, Z. J., Vysotski, E. S., Chen, C. J., Rose, J. P., Lee, J. & Wang, B.-C. (2000). *Protein Sci.* **9**, 2085–2093.
McPhillips, T. M., McPhillips, S. E., Chiu, H.-J., Cohen, A. E., Deacon, A. M., Ellis, P. J., Garman, E., Gonzalez, A., Sauter, N. K., Phizackerley, R. P., Soltis, S. M. & Kuhn, P. (2002). *J. Synchrotron Rad.* **9**, 401.
Matthews, B. W. (1966). *Acta Cryst.* **20**, 82–86.
Mitchell, C. M. (1957). *Acta Cryst.* **10**, 475–476.
North, A. C. T. (1965). *Acta Cryst.* **18**, 212–216.
Nurden, A. T. & Caen, J. P. (1975). *Nature (London)*, **255**, 720–722.
Okumura, T. & Jamieson, G. A. (1976). *Thromb. Res.* **8**, 701–706.
Otwinowski, Z. & Minor, W. (1997). *Methods Enzymol.* **276**, 307–326.
Peerdeman, A. F., Van Bommel, A. J. & Bijvoet, J. M. (1951). *Proc. Koninkl. Ned. Akad. Wet. B*, **54**, 16–19.
Pepinsky, R. & Okaya, Y. (1956). *Proc. Natl Acad. Sci. USA*, **42**, 286–292.
Ramachandran, G. N. & Raman, S. (1956). *Curr. Sci. (India)*, **25**, 348–351.
Ramaseshan, S. & Venkatesan, K. (1957). *Curr. Sci. (India)*, **26**, 352–353.
Rossmann, M. G. (1961). *Acta Cryst.* **14**, 383–388.
Terwilliger, T. C. (2000). *Acta Cryst.* D**56**, 965–972.
Terwilliger, T. C. & Berendzen, J. (1999). *Acta Cryst.* D**55**, 849–861.
Uff, S., Clemetson, J. M., Harrison, T., Clemetson, K. J. & Emsley, J. (2002). *J. Biol. Chem.* **277**, 35657–35663.
Ware, J. (1998). *Thromb. Haemost.* **79**, 466–478.
Watenpaugh, K. D., Sieker, L. C., Jensen, L. H., Legall, J. & Dubourdieu, M. (1972). *Proc. Natl Acad. Sci. USA*, **69**, 3185–3188.
Weeks, C. M., Blessing, R. H., Miller, R., Mungee, R., Potter, S. A., Rappleye, J., Smith, G. D., Xu, H. & Furey, W. (2002). *Z. Kristallogr.* **217**, 686–693.